Genomic Stability and Tumor Suppression by the APC/C Cofactor Cdh1

Irene García-Higuera[1,2], Eusebio Manchado[1], Pierre Dubus[3], Marta Cañamero[4], Juan Mendez[5], Sergio Moreno[2,6] and Marcos Malumbres[1,6]

1. *Cell Division and Cancer Group, Centro Nacional de Investigaciones Oncológicas (CNIO), Madrid, Spain*
2. *Instituto de Biología Molecular y Celular del Cáncer, CSIC/Universidad de Salamanca, Campus Miguel de Unamuno, 37007 Salamanca, Spain*
3. *EA2406 University of Bordeaux 2, Bordeaux, France*
4. *Comparative Pathology Unit, Centro Nacional de Investigaciones Oncológicas (CNIO), Madrid, Spain*
5. *DNA Replication Group, Centro Nacional de Investigaciones Oncológicas (CNIO), Madrid, Spain*
6. *Correspondence should be addressed to M.M. (e-mail: malumbres@cnio.es) or S.M. (e-mail: smo@usal.es).*

Keywords: Cdh1, Fzr1, Anaphase-Promoting Complex/Cyclosome, Cell Cycle, Mouse Models, Tumor Development, Genomic Instability

SUMMARY

The Anaphase Promoting Complex or Cyclosome (APC/C) is an ubiquitin protein ligase that, together with Cdc20 or Cdh1, targets cell cycle proteins for degradation. APC/C-Cdh1 specifically promotes protein degradation in late mitosis and G1. Mutant embryos lacking Cdh1 die at E9.5-E10.5 due to defects in the endoreduplication of trophoblast cells and placental malfunction. This lethality is rescued when Cdh1 is expressed in the placenta. Cdh1-deficient cells display inefficient proliferation and accumulate numeric and structural chromosomal aberrations, revealing a contribution of Cdh1 to the maintenance of genomic stability. Cdh1 heterozygous animals display increased susceptibility to spontaneous tumors suggesting that Cdh1 functions as a haploinsufficient tumor suppressor. These heterozygous mice also display several defects in behavior associated to increased proliferation of nervous stem cells. These results indicate that Cdh1 is required for preventing unscheduled proliferation of specific progenitor cells and protecting mammalian cells from genomic instability.

INTRODUCTION

Targeted protein destruction during the cell cycle is mostly achieved by ubiquitination and subsequent degradation of key cell cycle regulators, such as cyclins or cyclin-dependent kinase (Cdk) inhibitors[1,2]. Two major E3 ubiquitin ligases play a role in cell-cycle control, namely the SCF (Skp1/Cullin/F-box protein complex) and the Anaphase-Promoting Complex or Cyclosome (APC/C)[3-6]. Whereas SCF mostly controls the protein levels during S-phase, APC/C is thought to regulate mitotic proteins keeping their levels down after mitosis.

APC/C is composed of at least a dozen different structural subunits[5] and requires the association of one of two additional subunits that recognize and recruit specific substrates: Cdc20 and Cdh1 (encoded by the *Fzr1* gene in mammals). Cdc20 is thought to activate APC/C in early mitosis and Cdh1 in late mitosis and during G1 (Refs. 7,8). APC/C substrates include mitotic cyclins (cyclins A and B), mitotic kinases and their regulators (Aurora A/B, TPX2, survivin, Plk1, Nek2A), proteins involved in chromosome segregation such as securin, sororin and Sgo1, and replication proteins such as geminin or thymidine kinase. In addition, both Cdc20 and Cdh1 subunits are themselves substrates of APC/C-mediated degradation[2,5]. Skp2, a leucine-rich repeat F-box protein that recruits SCF targets is also an APC/C target[9,10]. On the other hand, Emi1, an APC/C inhibitor, is a target of the SCF complex, indicating strong interdependencies between APC/C and SCF in controlling cell cycle progression[11,12]. Some APC/C^{Cdh1} substrates such as cyclin A, cyclin B, Aurora A, Plk1, Tpx2, Cdc6 or Spk2, are overexpressed in human cancer correlating with chromosomal instability and poor prognosis[13].

To understand the physiological function of mammalian Cdh1, we have generated conditional knockout mice with a targeted mutation in the *Fzr1* locus. Complete inactivation of Cdh1 leads to embryonic lethality due to specific aberrations in placental structure. Ablation of Cdh1 also results in slight defects in the proliferation of embryonic fibroblasts

(MEFs) in culture and accumulation of chromosomal aberrations, suggesting a function for Cdh1 in preserving genome integrity. *Fzr1*(+/–) mice develop a variety of tumors late in life without losing the *Fzr1* wild-type allele, suggesting a haploinsufficient role for Cdh1 in tumor suppression. *Fzr1*(+/–) mice also display behavior abnormalities accompanied by hyperproliferation of specific progenitor cells in the brain.

RESULTS

Ablation of Cdh1 results in placental defects and embryonic lethality

Two recombinant *Fzr1*(+/loxfrt) ES clones (Fig. 1) were isolated (see Methods) and used to generate *Fzr1*(+/loxfrt) mice. Expression of the Flp and Cre recombinases produced the corresponding *Fzr1*(lox) and *Fzr1*(–) alleles (Fig. 1). *Fzr1*(+/–) mutants are fertile and do not develop gross anatomical abnormalities during the first year of life. We found the expected fractions of homozygous *Fzr1*(–/–) embryos until embryonic day (E)9.5 (Fig. 1d and Supplementary Table S1). However, by E10.5-E11.5, live *Fzr1*(–/–) embryos were present below the expected ratios (about 10% versus the expected 25%) and all these embryos appear growth retarded, as compared with wild-type littermates (Fig. 1e). No live *Fzr1*(–/–) embryo can be detected at E12.5 or later stages of development.

Histological examination of E10.5-E11.5 mutant embryos revealed normal morphogenesis and no signs of gross pathological lesions. In contrast, mutant placentas display a pale appearance (Fig. 1f) and a significant decrease in the size of the labyrinth and the number of fetal erytroblasts (Fig. 2a). In addition, trophoblast giant cells are underdeveloped and contain much smaller nuclei. These giant cells represent a unique population that undergoes repeated rounds of DNA synthesis without intervening mitoses (endoreduplication), which leads to formation of giant nuclei[14]. In wild-type placentas,

trophoblast giant cells contain up to 1500 N of DNA, with the majority of cells containing over 100 N of DNA. In contrast, the DNA content of *Fzr1*(–/–) trophoblasts is greatly reduced, with virtually all cells containing less than 100 N DNA (Fig. 2b) and suggesting a specific defect in endoreduplication.

To analyze whether these placental defects cause the lethality in *Fzr1*(–/–) embryos, we crossed *Fzr1*(lox/lox) mice with transgenic mice expressing the Cre recombinase under the Sox2 promoter[15]. In this model, Cre is expressed in most cells in the developing embryo, but not in the placenta. We found that this procedure fully rescued the embryonal lethality. The overall structure of the placenta and the number and ploidy of trophoblast giant cells is normal in *Fzr1*(Δ/Δ); Sox2-Cre(+/T) (not shown) and *Fzr1*(Δ/–); Sox2-Cre(+/T) embryos (Fig. 2a,b). In addition, we recovered viable *Fzr1*(Δ/Δ); Sox2-Cre(+/T) and *Fzr1*(Δ/–); Sox2-Cre(+/T) embryos at all points of development including E18.5 (Figure 2c) and postnatal day (P)3. In these embryos, the excision of exons 2 and 3 of Fzr1 by Cre is complete as detected by specific PCR amplification and immunublot analysis of cultured cells from these embryos (Supplementary Fig. S1).

Proliferative defects in Cdh1-deficient embryonic fibroblasts

Primary MEFs isolated from E10.5 *Fzr1*(–/–) embryos had no detectable Cdh1 expression (Fig. 1c). These mutant MEFs proliferated slightly slower than control MEFs (Fig. 3a) and contain a slight increase in the number of cells in S and G2/M phases of the cell cycle (Fig. 3b), suggesting a partial defect in these cell cycle stages. In addition, *Fzr1*(–/–) MEFs display a significantly higher susceptibility to the senescence-like crisis period after 2-3 passages (versus 4-5 passages in wild-type cells) following a 3T3 protocol (Fig. 3c). Most of these cultures form immortal clones although *Fzr1*(–/–) MEFs require 13-15 passages to

immortalize (versus 8-9 in wild-type cultures). These immortal *Fzr1*(–/–) cultures display similar proliferation defects than the corresponding mutant primary cells (Supplementary Fig. S2).

The absence of Cdh1 correlates with increased levels of Cdc20 (Fig. 3d), in agreement with a role for APC/C^{Cdh1} in the degradation of Cdc20[16,17]. In addition, the protein levels of cyclin A, but not other cyclins (data not shown), are significantly increased in Cdh1-*null* cells. Cyclin B protein levels are in fact decreased in asynchronous Cdh1-*null* cells. Since these cells display increased 4N DNA content, these results suggest either accumulation of non-mitotic (4N-G1) cells or a defective mitotic progression (see below). To further analyze the degradation of cell cycle regulators in non-proliferating *Fzr1*(–/–) MEFs, we removed growth factors from these cells. Many APC/C^{Cdh1} targets are efficiently degraded in wild-type cells after serum removal, including Cdc20, geminin, Aurora A (Fig. 3e), cyclin A or Aurora B (not shown). All these known APC/C^{Cdh1} targets are stabilized in serum-starved *Fzr1*(–/–) MEFs. In addition, the protein levels of the cell cycle regulator p16^{INK4a} are also stabilized in Cdh1-*null* cells (Fig. 3e), suggesting that deficient proliferation and earlier senescence in these mutant cells may be a consequence of increased cell cycle inhibitors.

Serum-starved *Fzr1*(–/–) MEFs entered S phase after serum stimulation with different kinetics than their wild-type counterparts (Fig. 4a). Sixty % of *Fzr1*(–/–) (versus 42% of wild-type) cells have entered S phase 18 h after serum stimulation. However, DNA replication is more inefficient in mutant cells since BrdU incorporation drops after this stage whereas 90% wild-type cells accumulate BrdU 24 h after stimulation with serum (Fig. 4a). Cdc20, Aurora A, and cyclin B levels are increased in Cdh1-*null* cells at all stages analyzed (Fig. 4b). Some APC/C^{Cdh1} substrates involved in DNA replication such as Cdc6 and, more dramatically, geminin are upregulated in Cdh1-null cells. Whereas cyclin E is slightly downregulated in mutant cells, cyclin A is also upregulated during S-phase. This upregulation of cyclin A and,

perhaps, cyclin B is likely to explain the slight increase in Cdk2 and Cdk1 kinase activities by 10-15 h after serum stimulation (Fig. 4c).

These alterations in Cdh1-null cells are accompanied by slightly reduced levels of both Mcm4 and Mcm5 in the chromatin, suggesting a defect in the formation of pre-replicative complexes. Interestingly, cyclin A is significantly bound to chromatin 15 h after stimulation with serum in *Fzr1*(–/–) but not *Fzr1*(+/+) cells, at a stage where BrdU incorporation peaks in these mutant cells (Fig. 4a). Thus, S-phase in Cdh1-deficient cells progresses with reduced loading of Mcm complexes to chromatin, increased concentration of the DNA replication inhibitor geminin, and premature Cdk1 activation; thus generating an inefficient environment for DNA replication.

Delayed mitosis and genomic instability in Cdh1-deficient cells

The mitotic drug nocodazole has similar efficiencies in arresting *Fzr1*(–/–) and *Fzr1*(+/+) cells, suggesting no defect in the spindle assembly checkpoint (Fig. 5a). However, whereas most wild-type cells have exited mitosis and undergone cytokinesis 2 h after drug removal, 60% of the *Fzr1*(–/–) MEFs remained with 4N content of DNA as measured by flow cytometry. After microscopic observation (Fig. 5b), we detected 35% of binucleated cells in *Fzr1*(–/–) versus 8.8% in *Fzr1*(+/+) cultures. Most *Fzr1*(–/–) cells lose the MPM2 phosphorylation signal, although with a delayed kinetics (about 30 min delay) as compared to wild-type cells (Fig. 5c-d). These results indicate that these *Fzr1*(–/–) MEFs remain as MPM2-negative, binucleated cells due to defective cytokinesis. This abnormal exit from mitosis may result from the inefficient degradation of Cdc20, cyclin B and Plk1 (Fig. 5e).

Most Cdh1 substrates are stabilized in Cdh1-null cells but eventually become degraded. We therefore tested whether Cdc20 or other APC/C complexes may cooperate to

degrade these proteins. Wild-type or Cdh1-null MEFs were transfected with specific small interference oligonucleotide RNAs (siRNAs) against Cdc20 or Cdc27, a structural subunit of APC/C. As indicated in Fig. 5f, the specific siRNAs provoke an incomplete but significant reduction in Cdc20 and Cdc27 protein levels. Most APC/C targets are stabilized after Cdh1 genetic deletion in this assay, both in asynchronous (0 h) and serum-starved (36 h) cells (Fig. 5f). Cdc27 downregulation phenocopies the effect of Cdh1 deletion suggesting that Cdh1 function is mediated by APC/C. Cyclin A2, Aurora B and geminin do not display significant stabilization after knocking down Cdc20 although Cdc20 may contribute to the degradation of cyclin B1, Aurora A and Plk1. This stabilization is not maintained in serum-starved cells, suggesting that Cdh1 is the major APC/C cofactor during G0.

The replicative defects and mitotic alterations in Cdh1-*null* cells do not prevent cell cycle progression since both primary (Fig. 3a) and immortal (Supplementary Fig. S2) cells proliferate in vitro. However, *Fzr1*(–/–) immortal cultures display a variety of aberrations including binucleated or multinucleated cells, metaphase plates with missaligned chromosomes in diploid or polyploid cells and multipolar spindles (Fig. 6a). Although these aberrations are not frequent in stably proliferating immortal cultures [6% of *Fzr1*(–/–) cells vs. 1% *Fzr1*(+/+) cells], they may contribute to increase the genomic instability. In fact, most *Fzr1*(–/–) immortal cultures display aberrant chromosome numbers (Fig. 6b) including highly aneuploid cells with 100-150 chromosomes. Chromosome breaks and non-disjuntion figures are also observed in near all metaphases analyzed (n=50) in five out of six *Fzr1*(–/–) clones (Fig. 6c). Spectral karyotipic analysis of these cells show a large variety of chromosome aberrations including 3, 4 or 5 copies of specific chromosomes, small chromosomal fragments and complex translocations affecting more than two chromosomes (Fig. 6d and Supplementary Fig. S3). Interestingly, 14% of metaphases analyzed in primary *Fzr1*(–/–)

cultures also contained chromosome breaks similarly to immortal clones (versus only 4.8% of metaphases in *Fzr1*(+/+) cells; data not shown).

Cdh1 functions as a haploinsufficient tumor suppressor *in vivo*

Histological analysis of several tissues in young (3-month) or adult (12-month) *Fzr1*(+/–) animals did not reveal any gross abnormalities (data not shown). In addition, *Fzr1*(+/–) mice develop less and smaller tumors than their wild-type littermates when subjected to a classical skin carcinogenesis protocol (Supplementary Fig. S4). These results indicate that tumor development is somehow impaired in young *Fzr1*(+/–) mice, probably as a consequence of decreased proliferation rates as observed in cultured cells. Interestingly, *Fzr1*(+/–) mice display a decreased survival (half-life of 22 months in mutant mice versus 30 months in wild-type mice) at later ages (Fig. 7a). Whereas 60% of *Fzr1*(+/+) mice are alive by 25-months of age, only 22% of *Fzr1*(+/–) survive by this age. Moreover, 25% of aged *Fzr1*(+/–) mice develop epithelial neoplasias that are not present in their wild-type counterparts (Fig. 7b-h). These tumors include adenocarcinomas and adenofibromas of the mammary gland (17% of females), and additional tumors in the lung, liver, kidney, testis and sebaceous gland (Supplementary Table S2). About 20% of *Fzr1*(+/–) mice develop B-cell lymphomas, a common type of tumor observed at the same frequency in wild-type mice. These data indicate that *Fzr1*(+/–) mice display a significant susceptibility mostly to epithelial tumors with age. As shown in Fig. 7i, the wild-type allele of *Fzr1* is retained in these epithelial tumors suggesting that Cdh1 may function as a haploinsufficient tumor suppressor in vivo.

Unscheduled proliferation of brain progenitors and behavior abnormalities in *Fzr1*(+/–) mice

Cdh1 is known to be highly expressed in the brain[18] and controls axonal growth and patterning in the mammalian brain[19]. The nervous system of *Fzr1*(+/–) mice does not display any gross abnormality either in the brain or peripheral tissues. However, we detected a significant increase in the proliferation rate of a specific fraction of cells in the subventricular zone (SVZ) of the brain (Fig. 8a). This region is the richest source of stem cells in the adult brain and contain a niche of Sox2- and Sox9-expressing stem cells that maintain neurogenesis[20,21]. As shown in Fig. 8a, the *Fzr1*(+/–)SVZ contains a high percentage of Ki67-positive cells and higher cellularity (Fig. 8a). However, the number of Sox2 or Sox9-positive cells is not significantly altered in this niche, suggesting an increased asymmetric proliferation that generates transient amplifying or mature cells negative for these two stem markers. We did not find differences in the structure of the *Fzr1*(+/–) hippocampus (data not shown), the other major neurogenic region in adult brain.

To further understand whether the reduced levels of Cdh1 may have physiological consequences in *Fzr1*(+/–) mice, we performed two different behavior tests in 1.5-year old mice. *Fzr1*(+/–) mice display a poor performance in the tightrope test, a widely used behavioural marker of neuromuscular coordination. As shown in Fig. 8b, wild-type mice successfully pass this test and they stay on a circular bar after three trials of 60 s of duration. However, about 55% of *Fzr1*(+/–) mice fall in the third trial ($p<0.01$) and about 10% of them still fall even after 5 trials, suggesting a neuromuscular vigor and coordination defect. *Fzr1*(+/–) mice also display a significantly ($p<0.015$) low recognition memory when compared to wild-type littermates in an object recognition assay (Fig. 8c). Whereas about 90% *Fzr1*(+/+) mice have a discrimination ratio higher than 0.5 (they dedicate more time to the 'new' object), 60% of *Fzr1*(+/–) are not able to discriminate the new object in the

conditions assayed. These results suggest a significant neuromuscular and memory defect in mice with reduced levels of Cdh1.

DISCUSSION

Cdh1 is not essential in budding or fission yeast[22-25], *C. elegans*[26] or *Drosophila*[27] suggesting that this protein is dispensable for the basic cell cycle. Genetic ablation of the mouse Cdh1-encoding gene, *Fzr1*, results in embryonic lethality accompanied by reduced flux of fetal blood in the placental labyrinth and defective endoreduplication of giant trophoblast cells. These defects are rescued when Cdh1 is specifically ablated in the embryo but not in the placenta, pointing to the placental abnormality as a cause of death in *Fzr1*(–/–) animals. At birth, no gross morphological abnormalities are found in these *Fzr1*(Δ/–); Sox2-Cre(+/T) newborns although preliminary results indicate that these mutant mice die few days after birth (data not shown).

Genetic elimination of Cdh1 in mammalian cells results in the accumulation of genomic aberrations linked to defects in the timing of DNA replication, exit from mitosis and cytokinesis. These defects correlate with increased levels of specific S-phase and mitotic regulators. Cyclin A and cyclin B are thought to be targeted for degradation by both APC/C^{Cdc20} and APC/C^{Cdh1}. Cdh1-*null* cells, however, display increased levels of cyclin A despite having increased levels of Cdc20, indicating that in cultured fibroblasts cyclin A levels are mainly controlled by APC/C^{Cdh1}. In addition, Cdc20 downregulation by RNA interference does not significantly stabilize cyclin A (Fig. 5f). On the other hand, cyclin B levels seem to be modulated by both Cdh1 and Cdc20, at least in asynchronous cells. Both cyclin A and cyclin B have S-phase promoting activity and their upregulation[28,29] and the concomitant increase in Cdk1 activity (Fig. 4) may result in early but inefficient DNA

replication. In addition, unscheduled replication in *Fzr1*(–/–) cells occurs with reduced cyclin E, reduced Mcm loading to the chromatin and increased levels of inhibitors such as $p16^{INK4a}$ and geminin resulting in inefficient DNA replication. Some of these replicative defects, as well as the delay in the exit from mitosis, have been observed using RNA interference and genetically-modified chicken cell lines[30,31].

Five of the Cdh1 targets upregulated in *Fzr1*(–/–) cells, namely Aurora A, Plk1, Cyclin A, Cyclin B and Cdc20, are part of the chromosomal instability signature of human tumors and display among the highest scores of correlation with poor prognosis in cancer[13,32]. Similarly, unbalanced expression of licensing DNA replication factors is also frequent in several tumor types[33,34]. These data suggest that loss of Cdh1 may induce gross genomic alterations during cell proliferation that can lead to tumor development. In fact, *Fzr1*(+/–) mice develop epithelial tumors such as mammary gland adenocarcinomas and adenofibromas that are not observed in wild-type mice. Moreover, these tumors maintain the *Fzr1* wild-type allele suggesting that Cdh1 is haploinsufficient for tumor suppression. Although the reduction in Cdh1 levels in young animals may result in inefficient proliferation of induced tumors (skin carcinogenesis protocol), the accumulation of genomic instability may facilitate tumor development in old mice, and may specifically promote the development of epithelial tumors that typically require a genomic instability component[35]. Similar results in CENP-E mutant mice have led to the hypothesis that genomic instability may act both as a tumor suppressor and an oncogene *in vivo*[36]. Also in agreement with these results, Cdh1 protein levels are decreased in some cancer cell lines[31] and re-expression of Cdh1 reduced tumor development by a malignant B-cell lymphoma cell line[37]. Although the human *Fzr1* gene contains a consensus CpG island in its promoter, hypermethylation of this region is not frequent in human tumors (I.G.H, S.M. and M.M., unpublished observations). Thus, the mechanism for the reduction in Cdh1 protein levels in some human tumors remains unidentified.

Cdh1 is known to be highly expressed in neurons[18] and Cdh1 silencing by RNA interference has specific effects on the morphology and growth of neuronal processes[19]. In addition, when Cdh1 is similarly depleted in postmitotic neurons and human neuroblastoma cells in culture, these cells exhibit apoptotic cell death[38]. This effect is accompanied by increased cyclin B protein levels and increased BrdU incorporation, suggesting that postmitotic neurons may be more susceptible to apoptotic cell death induced by unscheduled proliferation. Although *Fzr1*(+/–) mice do not display alterations in the structure of the nervous system, we have identified a specific set of cells in the SVZ that are particularly susceptible to reduced Cdh1 levels and display increased proliferation in mutant mice. Interestingly, these cells are hosted in a niche of cells positive for Sox2 and Sox9, two markers of neuronal stem cells[21,39]. These proliferative defects are accompanied by significant defects in neuromuscular coordination and defective learning in *Fzr1*(+/–) mice. Whether these behavior defects are a consequence of the alteration in SVZ progenitors is currently unknown. A deeper characterization of the role of Cdh1 in these progenitor cells will require specific deletion of the *Fzr1* gene to eliminate both alleles in these neuronal progenitors.

METHODS

Generation of *Fzr1*-targeted mice and histological analysis. The *Fzr1* gene-targeting construct was assembled by flanking exons 2 and 3 of the murine *Fzr1* locus with loxP sequences (Fig. 1a). A neomycin phosphotransferase (*neo*) cassette was used for positive selection of clones, whereas the thymidine kinase gene was used for negative selection with gancyclovir. Recombinant embryonal stem (ES) cells and clones were selected by Southern blot analysis using the probe “a” as indicated in Fig. 1a. Four out of 386 ES cell clones analyzed underwent homologous recombination at the *Fzr1* locus. Two recombinant ES cell

clones were used to generate *Fzr1*-deficient animals. Oligonucleotides and protocols for the genotyping of this colony of mice are available upon request to the authors.

TgpCAG-flpe [40] or TgCMV-Cre [41] transgenic mice were used for ubiquitous expression of Flp or Cre recombinases, respectively. To remove the neo^R selection marker we crossed *Fzr1*(+/loxfrt) mice with pCAG-Flpe transgenic animals[40] that express the Flp recombinase in a ubiquitous manner. To generate a null allele, we crossed *Fzr1*(+/lox) mice with a transgenic mice that express Cre recombinase in a ubiquitous manner[41]. Cre-mediated recombination between the two loxP sites eliminates exons 2 and 3 (Fig. 1a). Splicing from exon 1 to exon 4 sequences causes a frameshift in the open reading frame that results in the synthesis of a putative small polypeptide unrelated to Cdh1. Sox2-Cre mice that express Cre in embryonic but not in extra-embryonic tissues were reported previously [15]. All animals were maintained in a mixed 129/Sv (25%) x CD1 (25%) x C57BL/6J (50%) background. Mice were housed at the pathogen-free animal facility of the Centro Nacional de Investigaciones Oncológicas (Madrid) following the animal care standards of the institution. These animals were observed in a daily basis and sick mice were euthanized humanely in accordance with the Guidelines for Humane End Points for Animals used in biomedical research. Tumor latency has been considered equivalent to lifespan. For histological observation, dissected organs were fixed in 10%-buffered formalin (Sigma) and embedded in paraffin wax. Three- or five-micrometer-thick sections were stained with hematoxylin and eosin. Additional immunohistochemical examination of the tissues and pathologies analyzed was performed using specific antibodies against Ki67 (Master Diagnostica), Sox2 or Sox9 (Chemicon) or active caspase 3 (RyD Systems).

For quantification of DNA ploidy in trophoblast giant cells, placentas were collected from E10.5 wild-type and mutant embryos. 5 μm thick sections were cut and stained with Feulgen stain. Four wild-type and four *Fzr1*(–/–) placentas were analyzed. Images were

quantified using ImageJ software (National Institutes of Health, Bethesda, Maryland, USA, http://rsb.info.nih.gov/ij/). The ploidy of trophoblast giant cells was expressed relative to diploid decidual cells.

Cell culture and cytometry. Mouse embryonic fibroblasts (MEFs) were prepared from E10.5 embryos and cultured using standard protocols [42]. The whole embryo was minced and dispersed in 0.1% trypsin (20 min at 37°C). Cells were grown for two population doublings and then frozen. MEFs were subcultured 1:4 upon reaching confluence; each passage was considered to be two population doubling levels (PDLs). All cultures were maintained in Dulbecco's modified Eagle's medium (DMEM; Gibco) supplemented with 2 mM glutamine, 1% penicillin/streptomycin and 10% foetal bovine serum (FBS) or donor calf serum (CS).

Growth properties were analyzed using the classical 3T3 protocol. Every 3 days, cells were trypsinized, counted and 10^6 cells were plated per 10-cm plate. The relative number of cells is considered as a measure of the number of cells per passage related to the initial number of cells seeded per plate. DNA content was analyzed by flow cytometry (Becton-Dickinson). For growth-curve assays, cells were plated at 1×10^5 cells per well in 6-well plates. For cell cycle reentry, cells were starved in serum-free DMEM for 72 hr before being re-stimulated with 15% fetal bovine serum for the indicated times. To analyze mitotic progression, cells were pre-synchronized in G0 by serum starvation, released with 15% FBS in the presence of 0.2 μg/ml aphidicolin for 24 h, and then treated with 100 mM nocodazole (Sigma) for 12-14 h.

For RNA interference, *Fzr1*(+/+) and *Fzr1*(–/–) immortal MEFs were transfected with Cdc20 or Cdc27 siRNAs (Dharmacon) using Hyperfect (Dharmacon) as recommended by the manufacturers. Forty-eight hours after transfection, cells were either harvested (time 0) or serum starved for 36 h before whole lysates were isolated for protein analysis.

Immunodetection of total protein levels or chromatin-associated DNA replication proteins. Cells were washed twice with ice-cold PBS and lysed in NP-40 lysis buffer (150 mM NaCl, 1% NP-40, 50 mM Tris-HCl pH 8.0, 1 mM PMSF, 1 μg/ml Leupeptin, 25 μg/ml Aprotinin, 1 mM EDTA). After 30 min on ice, samples were vortexed (5 min at 4^{o}) and cleared by centrifugation. In addition, cells were subjected to a biochemical fractionation protocol that separates soluble and chromatin-bound proteins [43]. Proteins were separated on SDS-PAGE, transferred to nitrocellulose membranes (BioRad), probed using specific antibody and detected using fluorescent donkey (Rockland) or goat (Invitrogen) anti rabbit secondary antibodies followed detection using the Odyssey Infrared Imaging System (Li-Cor Biosciences). After transfer of the protein lysates, we probed nitrocellulose membranes with antibodies against Cdh1 (Neomarkers), p27^{Kip1} (Transduction Laboratories), Cdc6 and histone H4 (Upstate Signalling), Geminin, Cdc20 and cyclin A2 (Santa Cruz Biotechnology), cyclin B1 (Chemicon International), Aurora A, Aurora B, Cdc27 and Mek2 (Becton Dickinson), Plk1 (Zymed), Tpx2 and cyclin E (Abcam), phosphor-MPM2 and phosphor-histone H3 (Upstate Signalling), BrdU (Alexa Fluor 647 Conjugate; Molecular Probes) and β-Actin (Sigma). New anti-Mcm4 and anti-Mcm5 polyclonal sera were generated in rabbits using as antigens synthetic peptides corresponding to amino acids 23-36 in mouse Mcm4 and amino acids 593-606 in mouse Mcm5. Cdk2 and Cdk1 kinase activities were measured as described previously[44] using histone 1 as a substrate.

Scoring of chromosomal abnormalities. Metaphase preparations were made using 0.075 M KCl hypotonic treatment and methanol/acetic acid fixation from MEFs following 2 h treatment with 0.01 μg/ml colcemid. Slides were stained with 5% Giemsa in pH 6.8 buffer for 10 min. A total of 50 metaphases were scored in each clone analyzed. For spectral

karyotyping (SKY), painting probes for each chromosome were generated from flow-sorted mouse chromosomes using sequence-independent DNA amplification. Labeling was performed by incorporating four different dyes in a combination sequence that allows unique and differential identification of each chromosome. Slides were prepared from fixative-stored material and hybridized and washed using the SKY method according to the manufacturer's protocol (Applied Spectral Imaging, Migdal Ha-Emck, Israel). Chromosomes were counterstained with DAPI.

Behavior assays. The tightrope test was used as described previously[45]. Briefly, mice were placed on a bar of circular section (60 cm long and 1.5 cm diameter) and the test was considered successful when a mouse did not fall during a period of 60s in at least one out of five consecutive trials. Animals underwent the object recognition test following the protocol described previously[46] with minor modifications. Briefly, mice were placed in an experimental cage that consists in an open plastic box (73 cm-long x 55cm-wide x 32cm-high) with opaque walls. The two similar objects (objects X and Y) were plastic parallelepipeds and the dissimilar object (object Z) was a plastic bottle. The objects were placed along the long axis of the experimental cage, each 7 cm from each cage end. Mice were first exposed to the cage and to objects X and Y. After the familiarisation period, each mouse were released in the experimental cage with one of the old objects (object X) and a new one (object Z). After each exposure, the objects and the cage were wiped with ethanol 70% to eliminate odour cues. The size and weight of the objects used did not allow their movement or displacement by the animals. Animals were considered to show recognition activity when the head of the animal was less than 2 cm close to the object. The total time of recognition activity was scored manually using a stopwatch and registered.

Statistical analysis. Statistical analysis was performed using Student's t-test. All data are shown as mean with standard deviations (s. d.). Probabilities of $p < 0.05$ were considered significant.

ACKNOWLEDGEMENTS

We thank Gardenia Fresneda and Manuel Eguren for help with carcinogenic assays and molecular analysis; and Sheila Rueda and Blanca Velasco for their valuable help in the management of the mouse colony. We also thank Sagrario Ortega and the CNIO Transgenic Unit for their expertise in ES cell manipulations, and members of the CNIO Comparative Pathology Unit for histological and pathological processing, and the CNIO Cytogenetics Unit for their help in karyotype analysis. I.G.H. is supported by a Ramón y Cajal contract (Ministerio de Educación y Ciencia). E.M. is supported by a FIS fellowship (Ministerio de Sanidad). This work was supported by grants from the Association pour la Recherche contre le Cancer and the Région Aquitaine (to P.D.), Ministerio de Educación y Ciencia (SAF2004-05611 to I.G.H.; BFU2004-04886 to J.M.; BFU2005-03195 and GEN2003-20243-C08-05 to S.M.; and SAF2006-05186 to M.M.), the Consolider-Ingenio 2010 Programme (CSD2007-00015 to J.M. and S.M.; and CSD2007-00017 to M.M.), Comunidad de Madrid (OncoCycle Programme; S-BIO-0283-2006), Fundación Ramón Areces, and Fundación Médica Mutua Madrileña Automovilística (to M.M.); and Fundación Científica de la Asociación Española contra el Cáncer (to S.M. and M.M.).

AUTHOR CONTRIBUTIONS

I.G.H and E.M. performed most of experiments and J.M. carried out the analysis of chromatin-bound proteins. P.D. and M.C. performed the histological and pathological analysis of the samples. M.M. and S.M. designed and supervised the study and M.M. wrote the manuscript.

REFERENCES

1. Reed, S.I. Ratchets and clocks: the cell cycle, ubiquitylation and protein turnover. *Nat Rev Mol Cell Biol* **4**, 855-864 (2003).
2. Nakayama, K.I. & Nakayama, K. Ubiquitin ligases: cell-cycle control and cancer. *Nat Rev Cancer* **6**, 369-381 (2006).
3. Cardozo, T. & Pagano, M. The SCF ubiquitin ligase: insights into a molecular machine. *Nat Rev Mol Cell Biol* **5**, 739-751 (2004).
4. Harper, J.W., Burton, J.L. & Solomon, M.J. The anaphase-promoting complex: it's not just for mitosis any more. *Genes Dev* **16**, 2179-2206 (2002).
5. Peters, J.M. The anaphase promoting complex/cyclosome: a machine designed to destroy. *Nat Rev Mol Cell Biol* **7**, 644-656 (2006).
6. Acquaviva, C. & Pines, J. The anaphase-promoting complex/cyclosome: APC/C. *J Cell Sci* **119**, 2401-2404 (2006).

7. Pines, J. Mitosis: a matter of getting rid of the right protein at the right time. *Trends Cell Biol* **16**, 55-63 (2006).

8. Sullivan, M. & Morgan, D.O. Finishing mitosis, one step at a time. *Nat Rev Mol Cell Biol* **8**, 894-903 (2007).

9. Bashir, T., Dorrello, N.V., Amador, V., Guardavaccaro, D. & Pagano, M. Control of the SCF(Skp2-Cks1) ubiquitin ligase by the APC/C(Cdh1) ubiquitin ligase. *Nature* **428**, 190-193 (2004).

10. Wei, W. et al. Degradation of the SCF component Skp2 in cell-cycle phase G1 by the anaphase-promoting complex. *Nature* **428**, 194-198 (2004).

11. Vodermaier, H.C. APC/C and SCF: controlling each other and the cell cycle. *Curr Biol* **14**, R787-796 (2004).

12. Ang, X.L. & Harper, J.W. Interwoven ubiquitination oscillators and control of cell cycle transitions. *Sci STKE* **2004**, pe31 (2004).

13. Carter, S.L., Eklund, A.C., Kohane, I.S., Harris, L.N. & Szallasi, Z. A signature of chromosomal instability inferred from gene expression profiles predicts clinical outcome in multiple human cancers. *Nat Genet* **38**, 1043-1048 (2006).

14. Cross, J.C. How to make a placenta: mechanisms of trophoblast cell differentiation in mice--a review. *Placenta* **26 Suppl A**, S3-9 (2005).

15. Hayashi, S., Lewis, P., Pevny, L. & McMahon, A.P. Efficient gene modulation in mouse epiblast using a Sox2Cre transgenic mouse strain. *Mech Dev* **119 Suppl 1**, S97-S101 (2002).

16. Prinz, S., Hwang, E.S., Visintin, R. & Amon, A. The regulation of Cdc20 proteolysis reveals a role for APC components Cdc23 and Cdc27 during S phase and early mitosis. *Curr Biol* **8**, 750-760 (1998).

17. Shirayama, M., Zachariae, W., Ciosk, R. & Nasmyth, K. The Polo-like kinase Cdc5p and the WD-repeat protein Cdc20p/fizzy are regulators and substrates of the anaphase promoting complex in Saccharomyces cerevisiae. *Embo J* **17**, 1336-1349 (1998).

18. Gieffers, C., Peters, B.H., Kramer, E.R., Dotti, C.G. & Peters, J.M. Expression of the CDH1-associated form of the anaphase-promoting complex in postmitotic neurons. *Proc Natl Acad Sci U S A* **96**, 11317-11322 (1999).

19. Konishi, Y., Stegmuller, J., Matsuda, T., Bonni, S. & Bonni, A. Cdh1-APC controls axonal growth and patterning in the mammalian brain. *Science* **303**, 1026-1030 (2004).

20. Alvarez-Buylla, A. & Garcia-Verdugo, J.M. Neurogenesis in adult subventricular zone. *J Neurosci* **22**, 629-634 (2002).

21. Ferri, A.L. et al. Sox2 deficiency causes neurodegeneration and impaired neurogenesis in the adult mouse brain. *Development* **131**, 3805-3819 (2004).

22. Visintin, R., Prinz, S. & Amon, A. CDC20 and CDH1: a family of substrate-specific activators of APC-dependent proteolysis. *Science* **278**, 460-463 (1997).

23. Schwab, M., Lutum, A.S. & Seufert, W. Yeast Hct1 is a regulator of Clb2 cyclin proteolysis. *Cell* **90**, 683-693 (1997).

24. Yamaguchi, S., Murakami, H. & Okayama, H. A WD repeat protein controls the cell cycle and differentiation by negatively regulating Cdc2/B-type cyclin complexes. *Mol Biol Cell* **8**, 2475-2486 (1997).

25. Kitamura, K., Maekawa, H. & Shimoda, C. Fission yeast Ste9, a homolog of Hct1/Cdh1 and Fizzy-related, is a novel negative regulator of cell cycle progression during G1-phase. *Mol Biol Cell* **9**, 1065-1080 (1998).

26. Fay, D.S., Keenan, S. & Han, M. fzr-1 and lin-35/Rb function redundantly to control cell proliferation in C. elegans as revealed by a nonbiased synthetic screen. *Genes Dev* **16**, 503-517 (2002).

27. Sigrist, S.J. & Lehner, C.F. Drosophila fizzy-related down-regulates mitotic cyclins and is required for cell proliferation arrest and entry into endocycles. *Cell* **90**, 671-681 (1997).

28. Strausfeld, U.P. et al. Both cyclin A and cyclin E have S-phase promoting (SPF) activity in Xenopus egg extracts. *J Cell Sci* **109 (Pt 6)**, 1555-1563 (1996).

29. Moore, J.D., Kirk, J.A. & Hunt, T. Unmasking the S-phase-promoting potential of cyclin B1. *Science* **300**, 987-990 (2003).

30. Engelbert, D., Schnerch, D., Baumgarten, A. & Wasch, R. The ubiquitin ligase APC(Cdh1) is required to maintain genome integrity in primary human cells. *Oncogene* (2007).

31. Sudo, T. et al. Activation of Cdh1-dependent APC is required for G1 cell cycle arrest and DNA damage-induced G2 checkpoint in vertebrate cells. *Embo J* **20**, 6499-6508 (2001).

32. Perez de Castro, I., de Carcer, G. & Malumbres, M. A census of mitotic cancer genes: new insights into tumor cell biology and cancer therapy. *Carcinogenesis* **28**, 899-912 (2007).

33. Karakaidos, P. et al. Overexpression of the replication licensing regulators hCdt1 and hCdc6 characterizes a subset of non-small-cell lung carcinomas: synergistic effect with mutant p53 on tumor growth and chromosomal instability--evidence of E2F-1 transcriptional control over hCdt1. *Am J Pathol* **165**, 1351-1365 (2004).

34. Pinyol, M. et al. Unbalanced expression of licensing DNA replication factors occurs in a subset of mantle cell lymphomas with genomic instability. *Int J Cancer* **119**, 2768-2774 (2006).

35. DePinho, R.A. The age of cancer. *Nature* **408**, 248-254 (2000).

36. Weaver, B.A., Silk, A.D., Montagna, C., Verdier-Pinard, P. & Cleveland, D.W. Aneuploidy acts both oncogenically and as a tumor suppressor. *Cancer Cell* **11**, 25-36 (2007).

37. Wang, C.X., Fisk, B.C., Wadehra, M., Su, H. & Braun, J. Overexpression of murine fizzy-related (fzr) increases natural killer cell-mediated cell death and suppresses tumor growth. *Blood* **96**, 259-263 (2000).

38. Almeida, A., Bolanos, J.P. & Moreno, S. Cdh1/Hct1-APC is essential for the survival of postmitotic neurons. *J Neurosci* **25**, 8115-8121 (2005).

39. Nait-Oumesmar, B. et al. Activation of the subventricular zone in multiple sclerosis: evidence for early glial progenitors. *Proc Natl Acad Sci U S A* **104**, 4694-4699 (2007).

40. Rodriguez, C.I. et al. High-efficiency deleter mice show that FLPe is an alternative to Cre-loxP. *Nat Genet* **25**, 139-140 (2000).

41. Schwenk, F., Baron, U. & Rajewsky, K. A cre-transgenic mouse strain for the ubiquitous deletion of loxP-flanked gene segments including deletion in germ cells. *Nucleic Acids Res* **23**, 5080-5081 (1995).

42. Malumbres, M. et al. Mammalian cells cycle without the D-type cyclin-dependent kinases Cdk4 and Cdk6. *Cell* **118**, 493-504 (2004).

43. Mendez, J. & Stillman, B. Chromatin association of human origin recognition complex, cdc6, and minichromosome maintenance proteins during the cell cycle: assembly of prereplication complexes in late mitosis. *Mol Cell Biol* **20**, 8602-8612 (2000).

44. Quereda, V., Martinalbo, J., Dubus, P., Carnero, A. & Malumbres, M. Genetic cooperation between p21Cip1 and INK4 inhibitors in cellular senescence and tumor suppression. *Oncogene* **26**, 7665-7674 (2007).

45. Miquel, J. & Blasco, M. A simple technique for evaluation of vitality loss in aging mice, by testing their muscular coordination and vigor. *Exp Gerontol* **13**, 389-396 (1978).

46. Bevins, R.A. & Besheer, J. Object recognition in rats and mice: a one-trial non-matching-to-sample learning task to study 'recognition memory'. *Nat Protoc* **1**, 1306-1311 (2006).

Figure Legends

Figure 1 Generation of Cdh1 deficient mice. (**a**) Schematic representation of *Fzr1* alleles used in this study. The mouse *Fzr1* locus encoding Cdh1 contains 14 exons (boxes) spanning 12 kbp. Noncoding sequences (open boxes), loxP (open triangles) and frt (shaded triangles) sites are indicated. The neo^R cassette used for selection of homologous recombinant ES clones is indicated by an open arrow. The wild-type and different mutated *Fzr1* alleles used in this work are shown. (**b**) Southern-blot analysis of recombinant ES cell clones carrying the indicated alleles. The origin of the probes is indicated in (**a**) (probe a). Sizes of the diagnostic DNA fragments are indicated. (**c**) Analysis of Cdh1 expression in wild-type and mutant mice. β-actin was used as a loading control. (**d**) Appearance of viable *Fzr1*(+/+) and *Fzr1*(–/–) embryos at day 9.5 of gestation (E9.5). (**e**) By E11.5 most embryos are dead and the few viable embryos are growth retarded. (**f**) The corresponding extraembryonic tissues are smaller and display a reduced blood content by E11.5. Scale bars, 1 mm. Uncropped images of the scans are shown in Supplementary Information, Fig. S5.

Figure 2 Placental abnormalities in Cdh1 deficient embryos. (**a**) Histological sections of placentas derived from *Fzr1*(+/+) and *Fzr1*(–/–) embryos at day 10.5 of gestation. S, spongiotrophoblast; L, labyrinth. Fetal erythroid cells (empty arrowheads) are significantly reduced in mutant placentas. Trophoblast giant cell nuclei (marked by black arrowheads) are also smaller in mutant placentas. Both phenotypes are rescued in the *Fzr1*(Δ/–); Sox2-Cre(+/T) placentas. Original magnification: 40X (top panels); 400× (middle and bottom panels).(**b**) Ploidy distribution of trophoblast giant cells in wild-type, *Fzr1*(–/–) and *Fzr1*(Δ/–); Sox2-Cre(+/T) placentas. (**c**) Whereas *Fzr1*(–/–) embryos die before E11.5, *Fzr1*(Δ/–); Sox2-Cre(+/T) embryos in which Cdh1 is specifically eliminated in the embryo, but not in the

placenta, develop to term. Two representative pictures of *Fzr1*(+/Δ) and rescued *Fzr1*(Δ/–); Sox2-Cre(+/T) E18.5 embryos are shown. Scale bars, 200 μm in (**a**) and 1 mm in (**c**).

Figure 3 Cell proliferation in Cdh1 deficient embryos. (**a**) Growth curves of primary (passage 2) *Fzr1*(+/+) (open circles), *Fzr1*(+/–) (grey circles), and *Fzr1*(–/–) (filled squares) MEFs in complete medium with 10% or 2% fetal bovine serum. (**b**) DNA content profile of asynchronous *Fzr1*(+/+) and *Fzr1*(–/–) primary MEFs. Figures indicate the percentage of cells in each phase of the cell cycle. (**c**) These cells were maintained following a standard 3T3 protocol and cell numbers were scored in every passage. Although mutant MEFs enter the crisis period at earlier passages, all these genotypes become immortal after 13-15 passages (Supplementary Fig. 2). (**d**) Western-blot analysis of asynchronous *Fzr1*(+/+), *Fzr1*(+/–) and *Fzr1*(–/–) MEFs with antibodies directed against the indicated cell cycle proteins. (**e**) Western-blot analysis of the indicated cell cycle regulators in serum-starved *Fzr1*(+/+) and *Fzr1*(–/–) MEFs at the indicated time points after removal of growth factors. An antibody against β-actin was used for loading control in the blots. Data are mean ± s. d. Uncropped images of the scans are shown in Supplementary Information, Fig. S5.

Figure 4 Serum stimulation and DNA replication complexes in Cdh1 mutant cells. (**a**) MEFs were serum-starved for 72 h and forced to enter the cell cycle after stimulation with 15% fetal bovine serum and pulsed with BrdU. The percentage of BrdU positive cells is scored at different time points. By 18 h after stimulation with serum, *Fzr1*(–/–) MEFs display increased incorporation of BrdU in S-phase (right panels). However, by 24 h the percentage of cells that have incorporated BrdU is reduced compared to wild-type cells. (**b**) Immunodetection of the indicated cell cycle proteins in total lysates from *Fzr1*(+/+) and *Fzr1*(–/–) MEFs at the indicated time points after stimulation with serum. An additional sample from asynchronous

HeLa cells was used to identify the human proteins. β-actin was used as a loading control. (**c**) Total lysates were isolated at the indicated points and Cdk2 or Cdk1 complexes were immunoprecipitated (IP). Cdk2 and Cdk1 kinase activity (KA) was assayed using histone 1 as a substrate. M, mock immunoprecipitation. (**d**) Immunodetection of soluble and chromatin-bound proteins in *Fzr1*(+/+) and *Fzr1*(–/–) MEFs at the indicated time points after stimulation with serum. Mek2 (a cytosolic kinase) and histone H4 (a tightly-bound chromatin protein) are shown as controls of the fractionation protocol. Uncropped images of the scans are shown in Supplementary Information, Fig. S5.

Figure 5 Mitotic progression and exit in Cdh1 deficient cells. (**a**) DNA content of *Fzr1*(+/+) and *Fzr1*(–/–) MEFs after release of a nozodazole-induced prometaphase arrest. Whereas most wild-type cells become diploid after 2 h, a significant fraction of *Fzr1*(–/–) cells remain as 4N cells. (**b**) This is accompanied by a significant increase of *Fzr1*(–/–) binucleated cells in the nocodazole-released cultures. The percentage of binucleated cells was scored in a total of 250 *Fzr1*(+/+) and 250 *Fzr1*(–/–) cells. These cultures were stained with antibodies against α-tubulin (red), phosphor H3 (green) and with DAPI (blue). Scale bar, 10 μm. Data are mean ± s. d. (**c**) Quantification of phospho-MPM2 (a mitotic marker) levels after release from nocodazole showing a delay of about 30 min in the exit from mitosis. (**d**) MPM2/propidium iodide double staining of these cells showing a significant number of *Fzr1*(–/–) MPM2+ mitotic cells 1 h after nocodazole release. At this stage the MPM2 mark is lost or appears in diploid cells in the *Fzr1*(+/+) cultures. Some *Fzr1*(–/–) but not *Fzr1*(+/+) cells remain positive for MPM2 3 h after nocodazole release. (**e**) Immunodetection of the indicated cell cycle proteins in total lysates from *Fzr1*(+/+) and *Fzr1*(–/–) MEFs at the indicated time points after release from nocodazole. β-actin was used as a loading control. (**f**) Effect of Cdc20 or Cdc27 downregulation by RNA interference. *Fzr1*(+/+) and *Fzr1*(–/–) MEFs were transfected with

siRNAs against Cdc20 or Cdc27 and protein levels were analyzed in asynchronous cells (0 h) or 36h after serum removal. The indicated proteins were immunodetected using specific antibodies. Uncropped images of the scans are shown in Supplementary Information, Fig. S5.

Figure 6 Genomic defects in Cdh1 deficient cells. (**a**) Representative pictures of genomic and mitotic aberrations in immortal *Fzr1*(–/–) cultures. Cells were stained with antibodies against α-tubulin (red), and phospho-H3 (green). DAPI (blue) was also used in the top panels. (**b**) Quantification of chromosome numbers in *Fzr1*(+/+) and *Fzr1*(–/–) immortal cells. Diploid and tetraploid cells were grouped to indicate cells with complete sets of chromosomes (red bars) or carrying altered (aneuploid) genome composition. (**c**) Karyotypic analysis of *Fzr1*(–/–) immortal cells showing chromosome breaks and non-disjuntion structures (arrowheads). (**d**) Spectral karyotypic (SKY) analysis of immortal *Fzr1*(–/–) clones with genomic alterations including translocations and complex genomic compositions affecting the indicated chromosomes. Data are mean ± s. d. Scale bars, 10 μm.

Figure 7 Decreased survival and increased susceptibility to tumor development in Cdh1 mutant mice. (**a**), Survival curve of *Fzr1*(+/+) (n=19) and *Fzr1*(+/–) (n=51) mice. (**b**), Summary of tumors in these mice classified by cellular origin (**c-h**) Representative sections (hematoxylin and eosin staining at the indicated original magnification) of major pathologies in *Fzr1*(+/–) mice: (**c**) mammary gland adenocarcinoma (x25), (**d**) mammary gland fibroadenoma (x25); (**e**) lung adenoma (x200); (**f**) sebaceous gland adenoma (x25); (**g**) renal tubule adenoma (x100); (**h**) Plasmacytosis (x25). (**i**), Analysis of loss of heterozygosity in the following *Fzr1*(+/–) tumors: mammary gland adenocarcinoma (lane 1), sebaceous gland adenoma (2); lung adenocarcinoma (4), testis adenoma (5) and fibroadenoma (6). Lanes 3 and 7 correspond to control samples from healthy lungs in *Fzr1*(+/–) and *Fzr1*(+/+) mice,

respectively. The migration of wild-type (9.0 kbp) and mutant (7.5 kbp) alleles is shown. Scale bars, 200 μm.

Figure 8 Brain abnormalities and altered behaviour in mice heterozygous for the Cdh1 mutation. (**a**) Representative pictures of brain sections in *Fzr1*(+/+) and *Fzr1*(+/–) mice stained with hematoxylin and eosin (H&E), or antibodies against Ki67, Sox2 or Sox9. The situation of the subventricular zone (SVZ) analyzed is indicated by small squares. The quantification of Ki67+ (grey bars) or total number (black bars) of cells in the SVZ niche close to the ependyma of these *Fzr1*(+/+) and *Fzr1*(+/–) mice is shown (as number of cells per brain coronal section). Original magnification is 50X (H&E images) or 400X (immunostainings). Scale bars, 1 mm (top panels) or 50 μm (mid or bottom panels). (**b**) Performance of *Fzr1*(+/+) and *Fzr1*(+/–) mice in the tightrope test. The percentage of mice that successfully pass the test after three trials is shown in the left panel. The percentage of mice that fail in the different trials is shown in the right panel. (**c**) Performance of *Fzr1*(+/+) and *Fzr1*(+/–) mice in the object recognition test. The average discrimination ratio is shown for *Fzr1*(+/+) and *Fzr1*(+/–) males and females (left panel). The percentage of mice with a discriminatio ratio higher than 0.5 is shown in the right panel. Data are mean ± s. d. Asterisks indicate statistically significant differences at the confidence level shown.

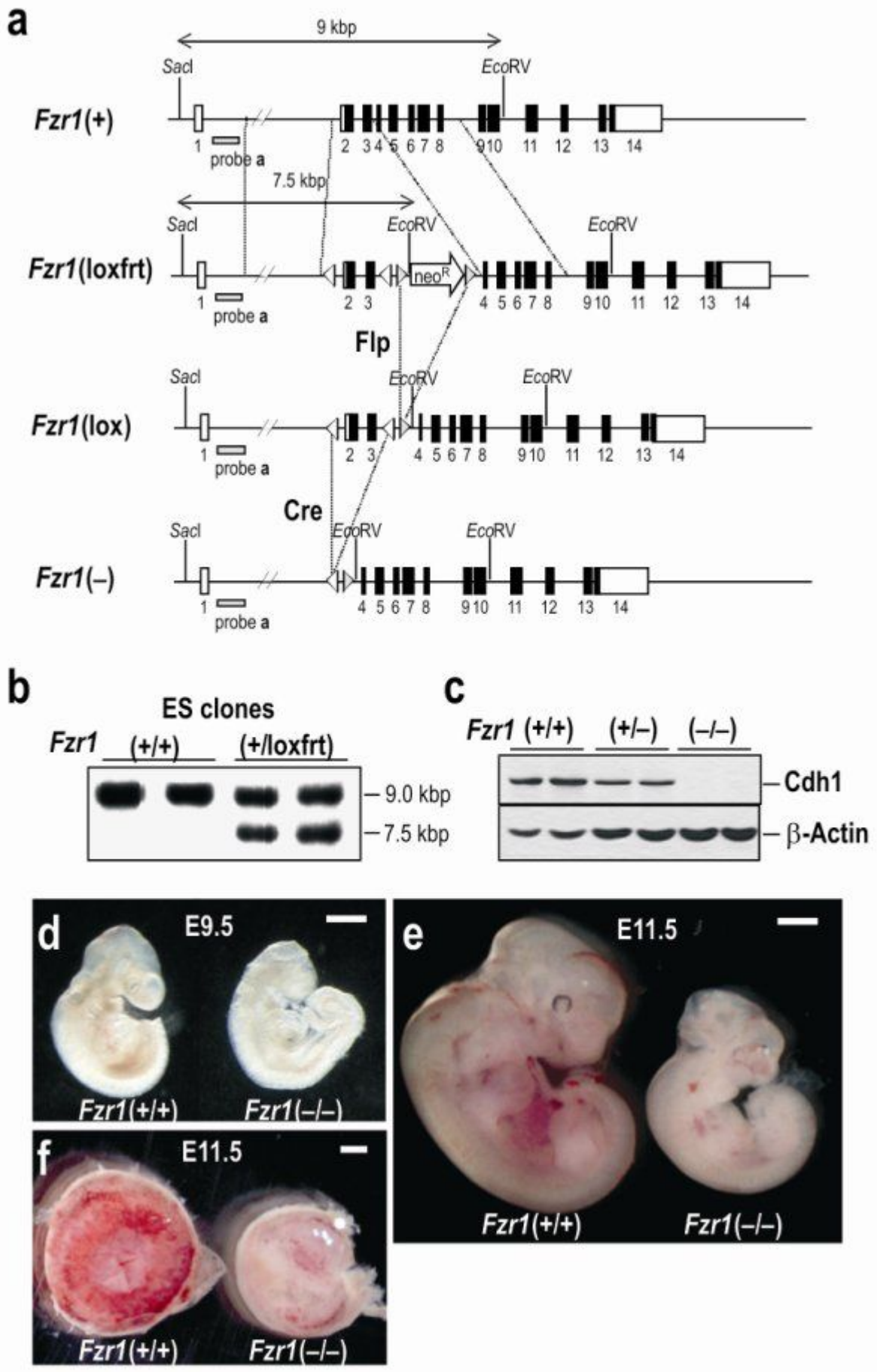
a
9 kbp
SacI
EcoRV
Fzr1(+)
1
probe a
2 3 4 5 6 7 8
9 10
11
12
13
14
7.5 kbp
Fzr1(loxfrt)
neoR
Flp
Fzr1(lox)
Cre
Fzr1(–)
b
ES clones
Fzr1
(+/+)
(+/loxfrt)
9.0 kbp
7.5 kbp
c
Fzr1 (+/+)
(+/–)
(–/–)
Cdh1
β-Actin
d
E9.5
Fzr1(+/+)
Fzr1(–/–)
e
E11.5
f
E11.5

Figure 1

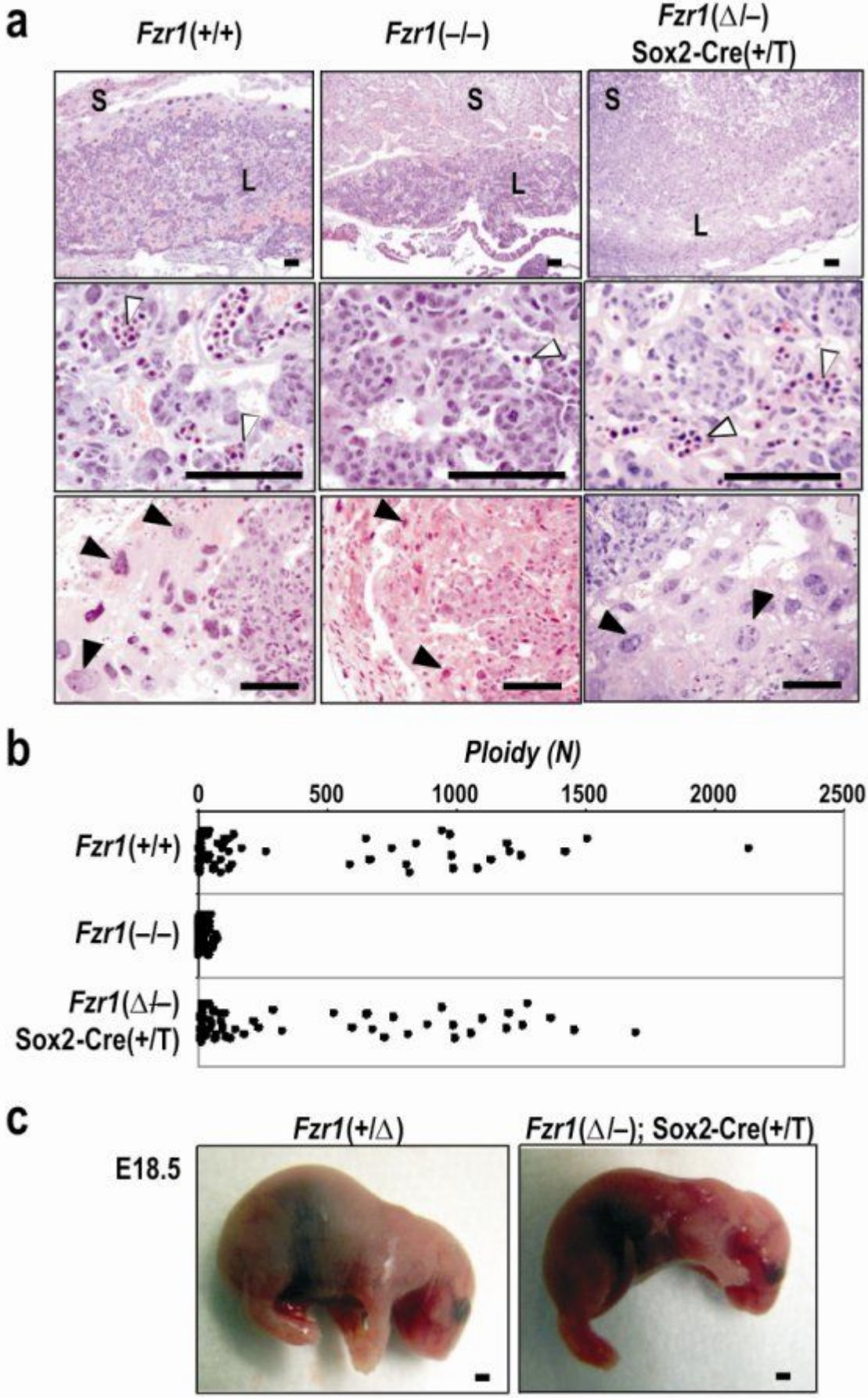
a
Fzr1(+/+)
Fzr1(–/–)
Fzr1(Δ/–)
Sox2-Cre(+/T)
S
L
b
Ploidy (N)
0
500
1000
1500
2000
2500
Fzr1(+/+)
Fzr1(–/–)
Fzr1(Δ/–)
Sox2-Cre(+/T)
c
Fzr1(+/Δ)
Fzr1(Δ/–); Sox2-Cre(+/T)
E18.5

Figure 2

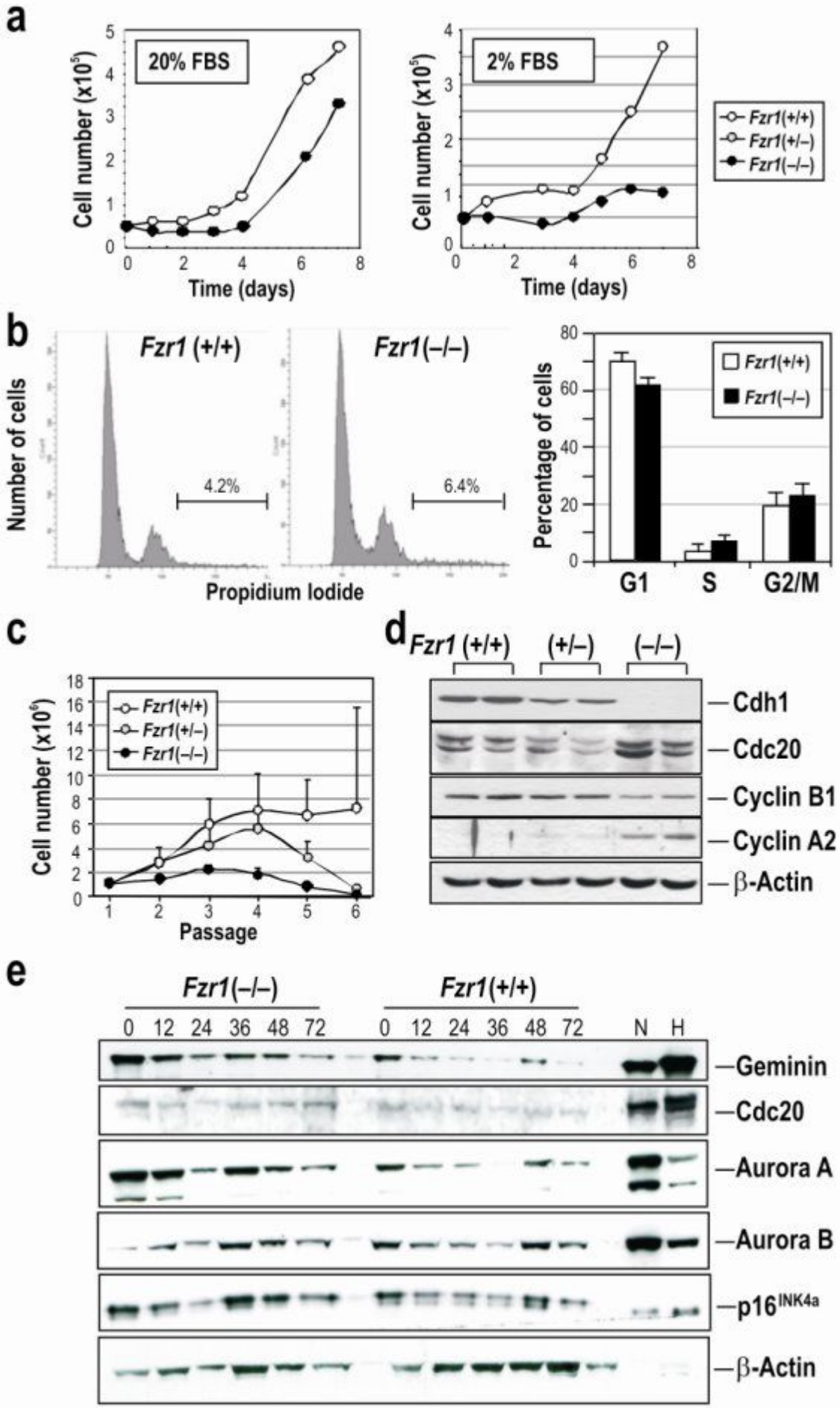
a
20% FBS
2% FBS
Cell number (x10^5)
Time (days)
Fzr1(+/+)
Fzr1(+/–)
Fzr1(–/–)
b
Fzr1 (+/+)
Fzr1(–/–)
Number of cells
4.2%
6.4%
Propidium Iodide
Percentage of cells
G1
S
G2/M
c
Cell number (x10^6)
Passage
d
Fzr1 (+/+)
(+/–)
(–/–)
Cdh1
Cdc20
Cyclin B1
Cyclin A2
β-Actin
e
Fzr1(–/–)
Fzr1(+/+)
0 12 24 36 48 72
N H
Geminin
Cdc20
Aurora A
Aurora B
p16INK4a
β-Actin

Figure 3

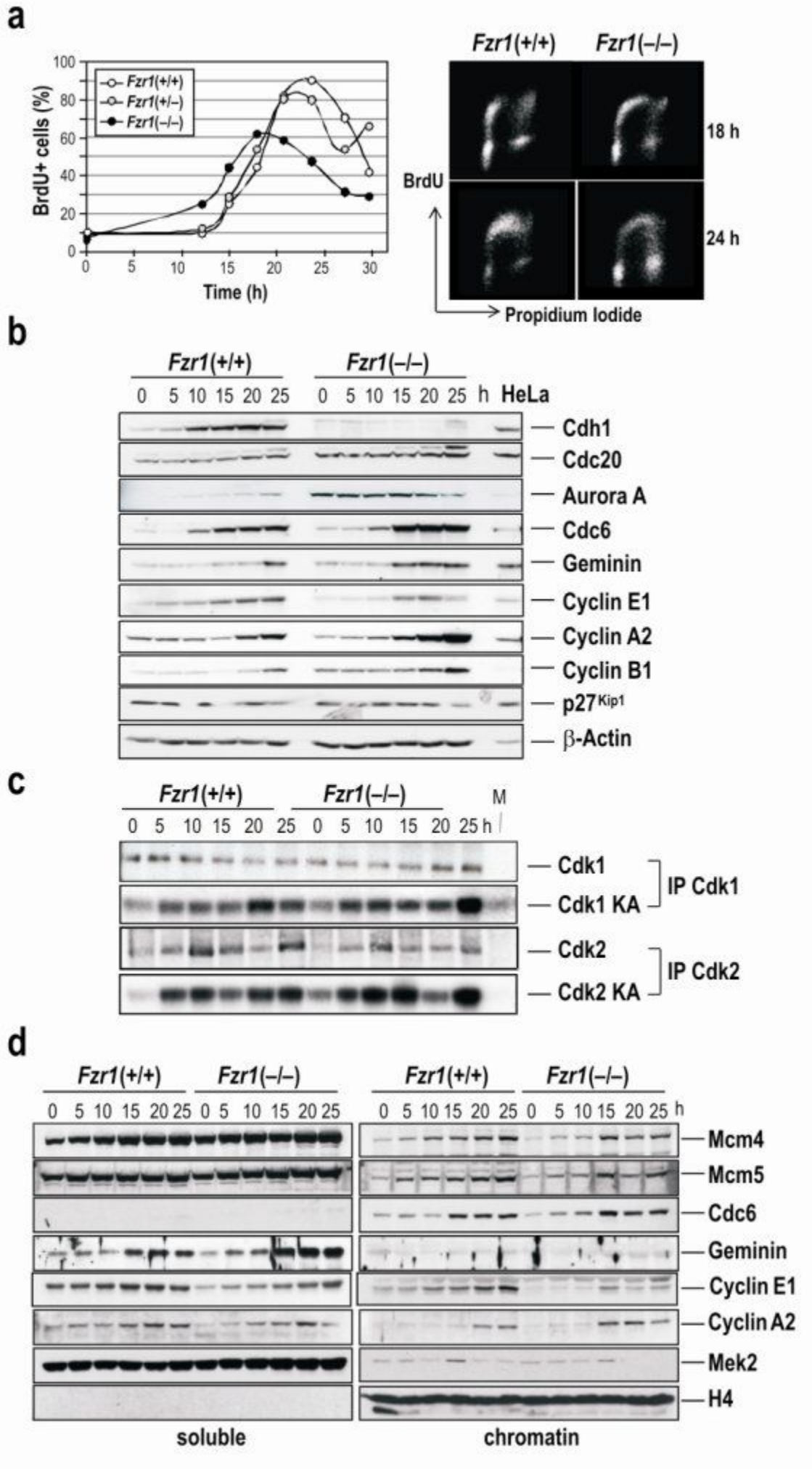
a
Fzr1(+/+)
Fzr1(+/–)
Fzr1(–/–)
BrdU+ cells (%)
Time (h)
Fzr1(+/+)
Fzr1(–/–)
18 h
24 h
BrdU
Propidium Iodide
b
Fzr1(+/+)
Fzr1(–/–)
0 5 10 15 20 25 0 5 10 15 20 25 h HeLa
Cdh1
Cdc20
Aurora A
Cdc6
Geminin
Cyclin E1
Cyclin A2
Cyclin B1
p27Kip1
β-Actin
c
Fzr1(+/+)
Fzr1(–/–)
M
0 5 10 15 20 25 0 5 10 15 20 25 h
Cdk1
Cdk1 KA
IP Cdk1
Cdk2
Cdk2 KA
IP Cdk2
d
Fzr1(+/+)
Fzr1(–/–)
Fzr1(+/+)
Fzr1(–/–)
0 5 10 15 20 25 0 5 10 15 20 25 0 5 10 15 20 25 0 5 10 15 20 25 h
Mcm4
Mcm5
Cdc6
Geminin
Cyclin E1
Cyclin A2
Mek2
H4
soluble
chromatin

Figure 4

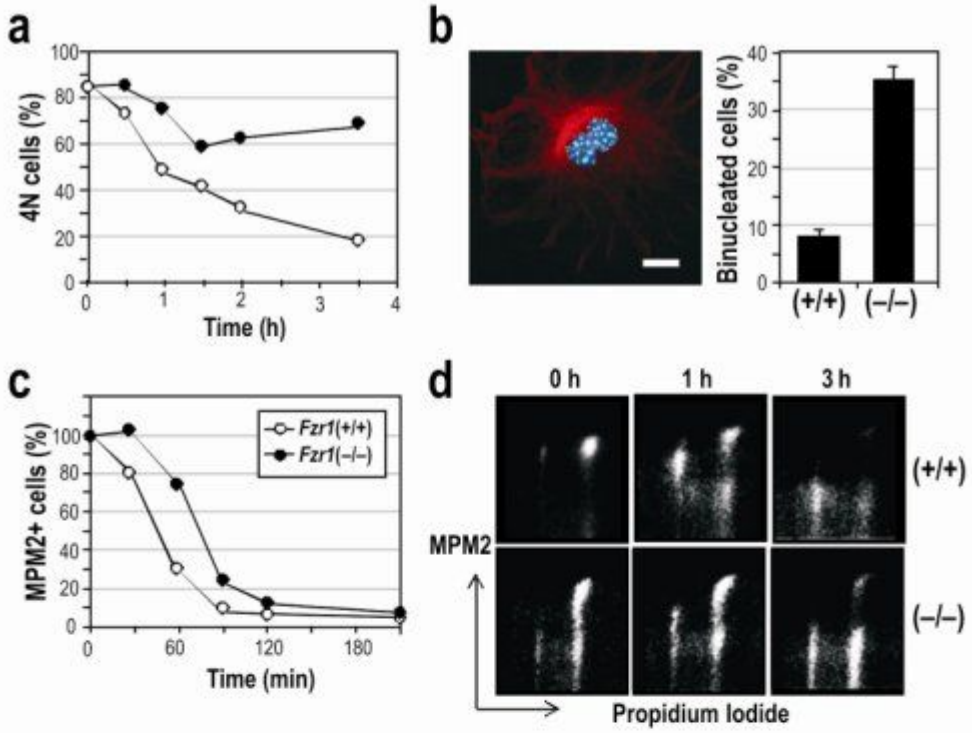
a
4N cells (%)
Time (h)
b
Binucleated cells (%)
(+/+)
(–/–)
c
MPM2+ cells (%)
Fzr1(+/+)
Fzr1(–/–)
Time (min)
d
0 h
1 h
3 h
(+/+)
(–/–)
MPM2
Propidium Iodide

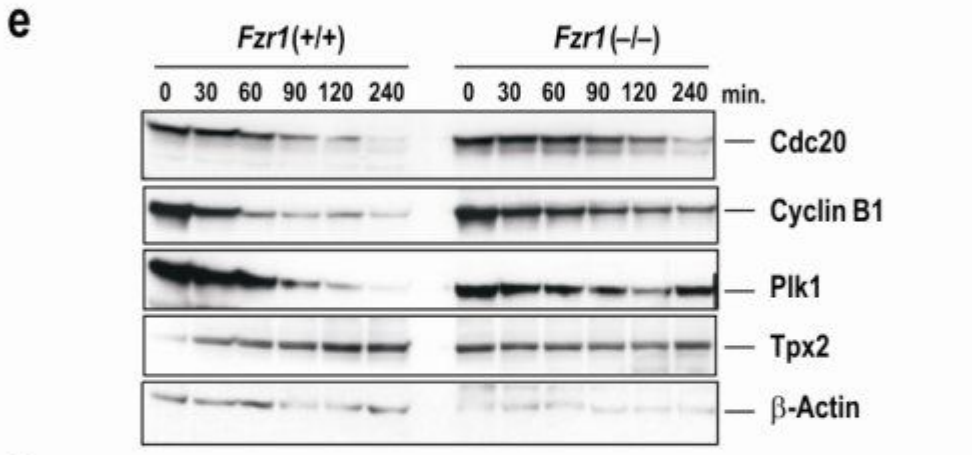
e
Fzr1(+/+)
Fzr1(–/–)
0 30 60 90 120 240 min.
Cdc20
Cyclin B1
Plk1
Tpx2
β-Actin

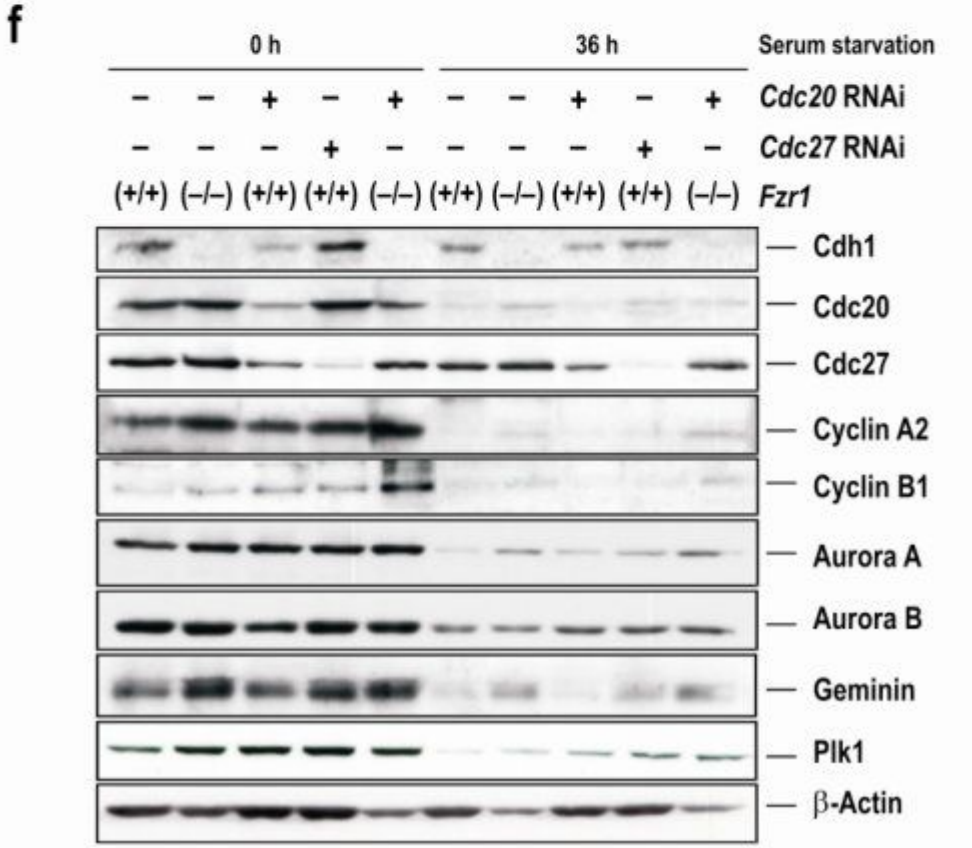
f
0 h
36 h
Serum starvation
Cdc20 RNAi
Cdc27 RNAi
Fzr1
Cdh1
Cdc20
Cdc27
Cyclin A2
Cyclin B1
Aurora A
Aurora B
Geminin
Plk1
β-Actin

Figure 5

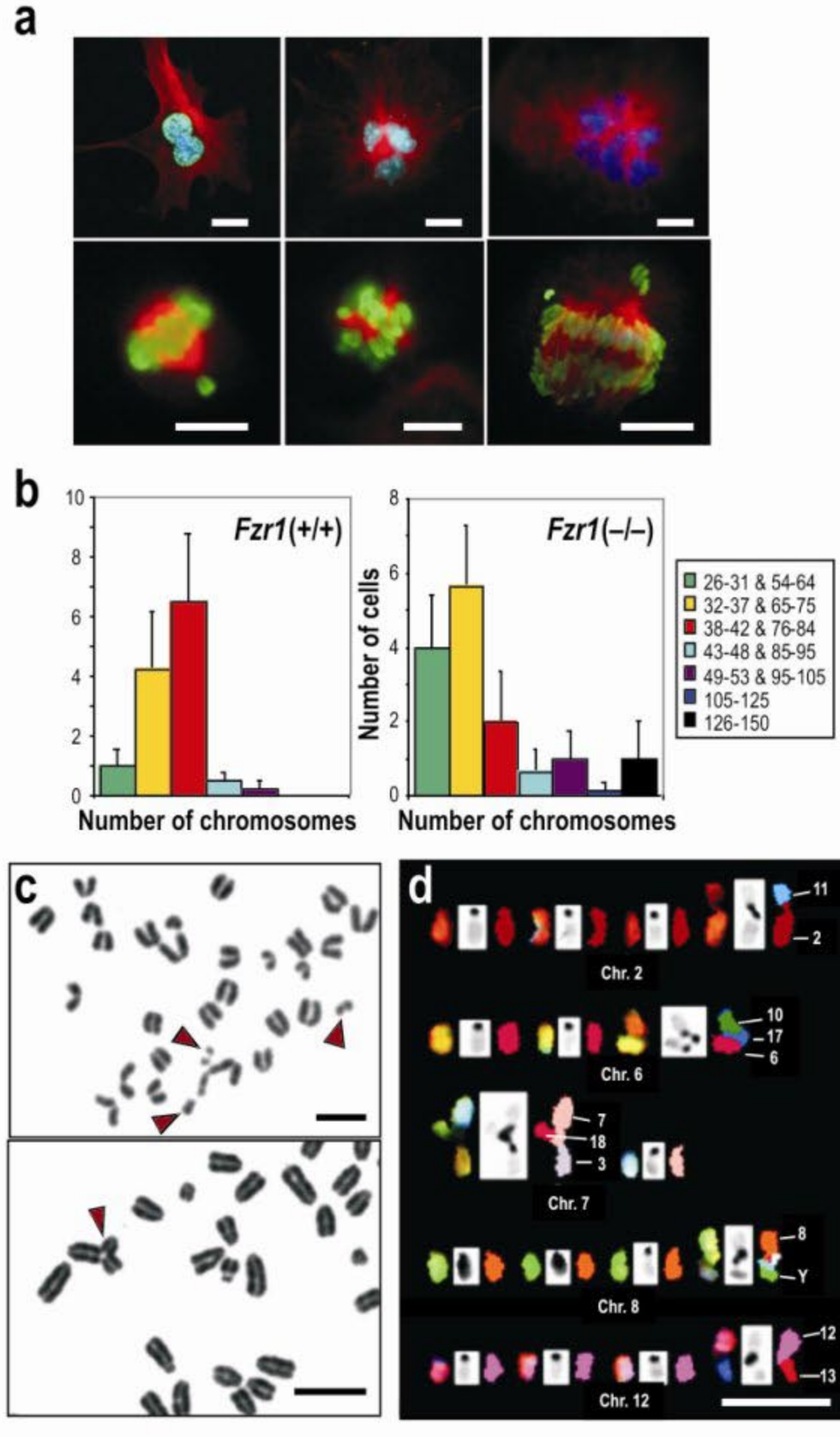
a
b
Fzr1(+/+)
Fzr1(–/–)
Number of cells
Number of chromosomes
Number of chromosomes
26-31 & 54-64
32-37 & 65-75
38-42 & 76-84
43-48 & 85-95
49-53 & 95-105
105-125
126-150
c
d
Chr. 2
Chr. 6
Chr. 7
Chr. 8
Chr. 12

Figure 6

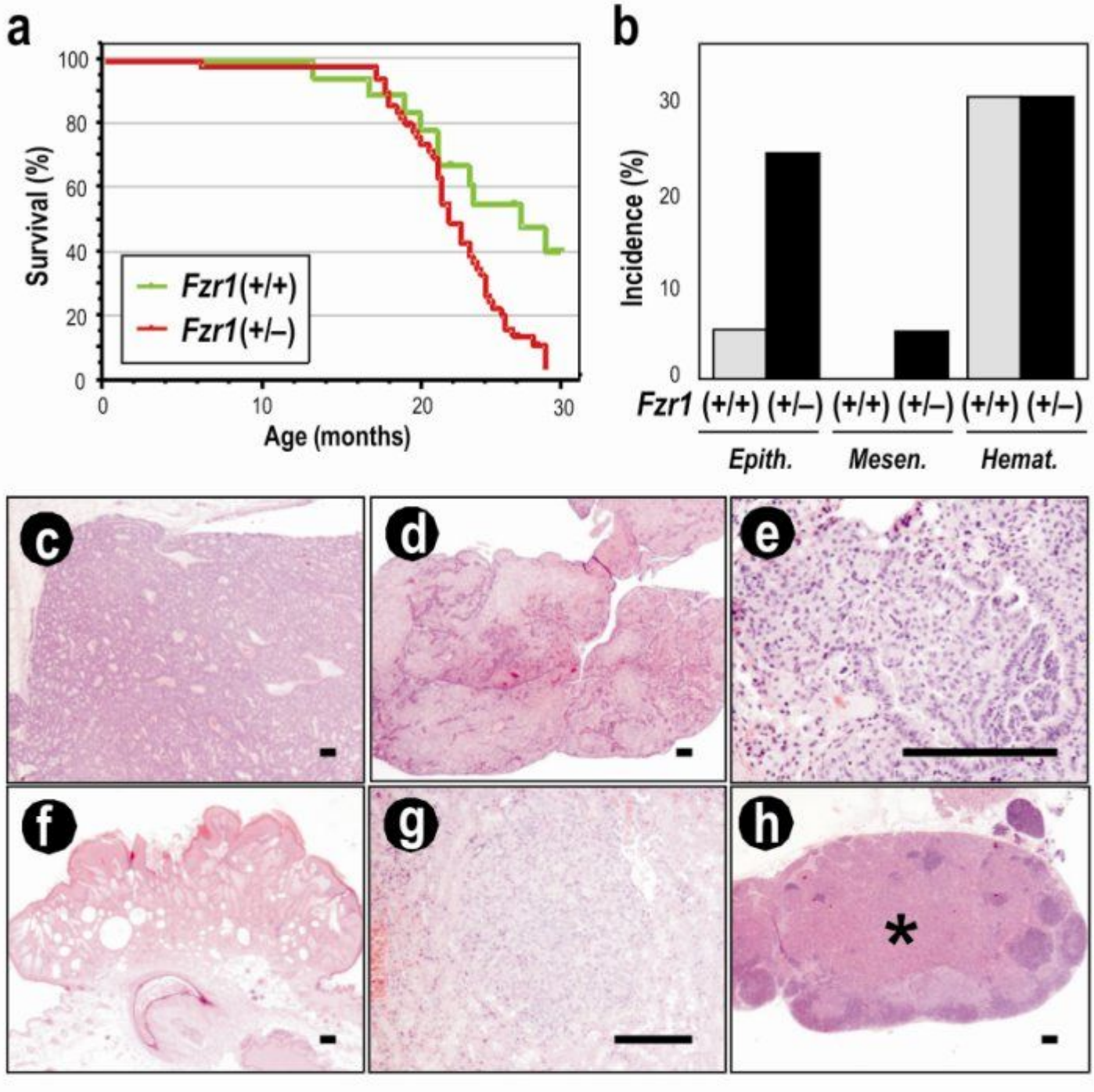
a
Survival (%)
100
80
60
40
20
0
0
10
20
30
Age (months)
Fzr1(+/+)
Fzr1(+/–)
b
Incidence (%)
30
20
10
0
Fzr1 (+/+) (+/–) (+/+) (+/–) (+/+) (+/–)
Epith.
Mesen.
Hemat.
c
d
e
f
g
h
*
i
Fzr1(+/–)
Fzr1(+/+)
T
N
T
N
1 2 3 4 5 6 7
9.0 kbp
7.5 kbp

Figure 7

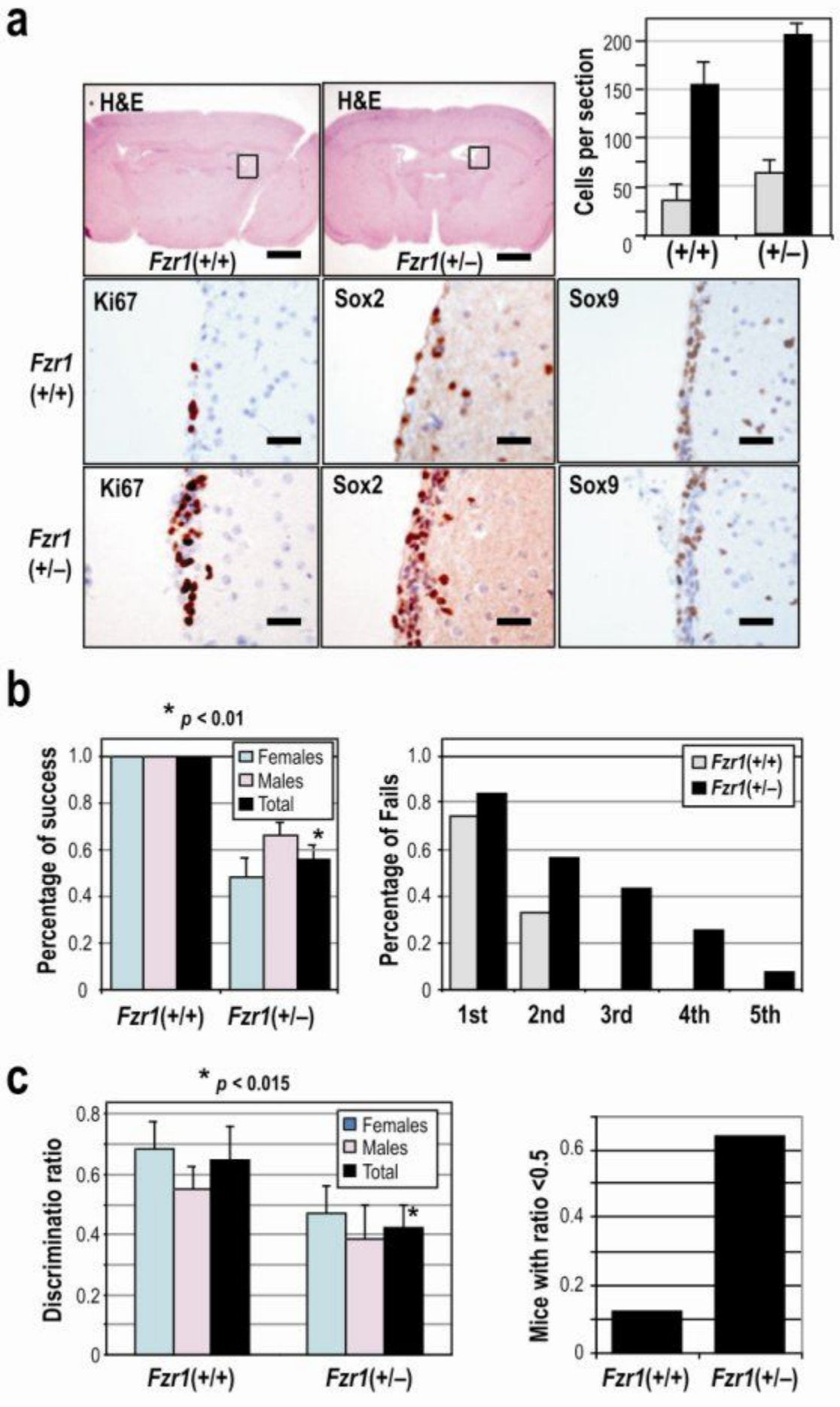
a
H&E
H&E
Fzr1(+/+)
Fzr1(+/–)
Cells per section
200
150
100
50
0
(+/+)
(+/–)
Ki67
Sox2
Sox9
Fzr1 (+/+)
Ki67
Sox2
Sox9
Fzr1 (+/–)
b
* p < 0.01
Percentage of success
1.0
0.8
0.6
0.4
0.2
0
Females
Males
Total
*
Fzr1(+/+)
Fzr1(+/–)
Percentage of Fails
1.0
0.8
0.6
0.4
0.2
0
Fzr1(+/+)
Fzr1(+/–)
1st
2nd
3rd
4th
5th
c
* p < 0.015
Discriminatio ratio
0.8
0.6
0.4
0.2
0
Females
Males
Total
*
Fzr1(+/+)
Fzr1(+/–)
Mice with ratio <0.5
0.6
0.4
0.2
0
Fzr1(+/+)
Fzr1(+/–)

Figure 8